EMI/PMC 2012
2012 Joint Conference of the Engineering Mechanics Institute and the
11th ASCE Joint Specialty Conference on Probabilistic Mechanics and Structural Reliability
June 17-20 2012, Notre Dame, IN

Fracture Behavior of ASTM A633 Steel Plate Specimens with Edge Crack at Tensile Test

Masood Hajali[1], Caesar Abishdid[2]
[1]PhD Candidate, Dept. of Civil and Environmental Engineering, Florida International University, Miami, FL 33174, Phone: (954)849-0078, E-mail: mhaja002@fiu.edu
[2]Director of External Programs, College of Engineering and Computing, Florida International University, Miami, FL 33174, Phone: (305)348-3813, E-mail: abishdid@fiu.edu

Abstract

The tensile test is an important and widely used test to determine the mechanical properties of steel materials. In tensile test, a specimen is pulled and specimen deformation and applied load is recorded until its fracture to draw load-displacement curve. This work presents an experimental study of the mechanical behavior of the ASTM A633 grade high-strength low-alloy (HSLA) steel plate specimens with edge crack at the middle during the tensile test. Experimental analysis is used to analyze the load-displacement curve, and fracture surface around the crack. Also Finite Element Method (FEM) is used to see the J-integral curve for various crack lenghs. A633 HSLA steel plate specimens are tested in FIU Material Laboratory using a high capacity universal testing machine with various crack lengths. Phenom microscope is used to get the best images from the crack tip surface of the fractured samples. This paper evaluates the effect of crack length on the load-displacement curve and also fracture behavior of steel specimens is investigated after tensile tests. Results show that with crack length increasing, yield strength, the ultimate tensile strength, and fracture stress show a decreasing trend. Also, fracture will occur in the angle of principle shear stress.

1 Introduction

The tensile test is an important and widely used test to determine the mechanical properties of steel materials. In tensile test, a specimen is pulled and specimen deformation and applied load is recorded until its fracture to draw stress-strain curve. Stress-strain diagram indicates the yield strength, ultimate tensile strength, elastic modulus, and ductility of the material. Metals including carbon steel have a linear stress-strain relationship up to the yield point. In some steels the stress falls after the yield point. After the yield point, steel will undergo a period of strain hardening, in which the stress increases again with increasing strain up to the ultimate strength. If the material is unloaded at this point, the stress-strain curve will be parallel to that portion of the curve between the origin and the yield point [1].

Tension tests provide information on the strength and ductility of materials under uniaxial tensile stresses. This information may be useful in comparisons of materials, alloy development, quality control, and design under certain circumstances. The results of tension tests of specimens machined to standardized dimensions from selected portions of a part or material may not totally represent the strength and ductility

properties of the entire end product or its in-service behavior in different environments. These test methods are considered satisfactory for acceptance testing of commercial shipments. The test methods have been used extensively in the trade for this purpose.

Due to the non-uniform stress-strain relationship and plastic variables related to the mechanical behavior of steel materials is important to evaluate the changes in the geometric configuration of specimen till fracture stage. Fracture is the result of an applied stress and this stress can be tensile, compression, shear or torsion. There are two fracture modes possible, ductile and brittle depending on the ability of the material to experience plastic deformation. Obviously we do not want failures to occur. However, if they are inevitable, it is far better that we have some warning instead of a sudden catastrophic failure with no warning. When a material does strain significantly before failure, it will exhibit a ductile fracture. In the 1920s, Griffith proposed that fracture occurs when the theoretical cohesive strength is exceeded at the tip of one of the numerous flaws existing in most materials.

Kardomateas (1986) found out that for the usual symmetric singly grooved plane strain specimens in tension the slip line field consists of two lines at 45^0 intersecting the tip of the groove. In the asymmetric case only a single shear zone exists as shown in Figure 1. This case shows less ductility that the symmetric case because the crack is advancing into prestrained material along the shear band rather than the new material encountered by a crack advancing between two symmetrical shear zones. Fractographic observations of deformation during crack extension in the asymmetric, mixed Mode I and II specimens suggests a mechanism of fracture followed by sliding off along two slip planes; a larger amount of sliding off occurring in the low flank. The usual symmetric case suggests alternating shear and fracture and in some cases the microscopic surface is characterized by zig-zagging [2].

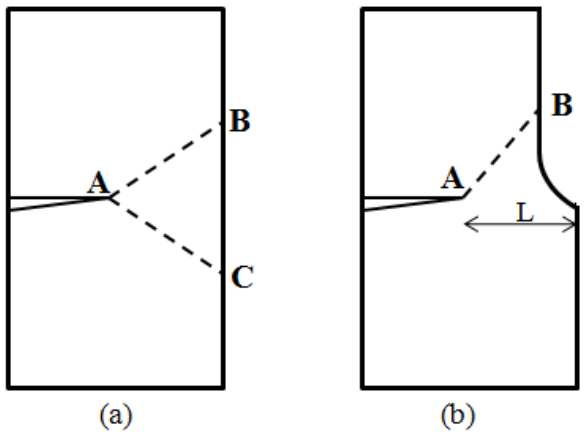

Figure 1. (a) Symmetric, (b) Asymmetric shear band configuration from cracks

The aim of this paper is to present an experimental analysis and a numerical method of the mechanical and fracture behavior during the tensile test experienced by ASTM633 HSLA specimens with edge crack in plane strain condition.

2 Stress, Strain, and Displacement

The main purpose of fracture mechanics is to determine the status of cracks in different loading conditions. Stress, strain, displacement, and energy fields are required to obtain a driving force for crack growth. Stress Intensity Factor (SIF) and *J*-integral are two important concepts of crack problems. SIF is used to quantify the stress field around the crack tip. Many methods have been developed to determine the

stress intensity factor. One of these methods to calculate the stress intensity factor is *J*-integral. The material can be cracked in three different modes including opening, shearing, and tearing mode. The first mode is related to the tensile stress which is orthogonal to the page, and is called opening mode. The second mode is applied in the same way as shear stress on the page, and is called shearing or sliding mode. The third mode which includes out-of-plane shear stress of the crack is called tearing mode. Other situations of the loading are combinations of these three modes. If a node is considered with distance *r* and angle of α with the x-axis in the vicinity of the crack edge, then the stress field in this node is calculated according to the Irwin method in different crack modes. Therefore, stress field in the crack tip for linear elastic materials is calculated by Equation (1):

$$\sigma_{ij} = \frac{K}{\sqrt{2\pi r}} f_{ij}(\theta) \tag{1}$$

K parameter is the SIF for different modes in the crack tip, and shown K_I, K_{II}, and K_{III} are for the first, second and third mode. Values of these coefficients are determined according to the dimensions and loading condition of the problem. Therefore, the SIF relationship is calculated from the analysis of the geometrical and loading condition. K_I, K_{II}, and K_{III} are physically the intensity of force transfer at the crack tip due to creation of the crack in the material. SIF plays an important role as a failure parameter. Rice (1968) also showed that this integral has linear elastic attitude with the energy release rate and was independent of the path around a crack. The two-dimensional *J*-integral was defined as Equation (2):

$$J = \oint_{\Gamma} W dy - T_i \frac{\partial u_i}{\partial x} ds \tag{2}$$

where *W* is strain energy density, and *u* is the displacement vector. The strain energy density is given by:

$$W = \int_0^{\varepsilon_{ij}} \sigma_{ij} d\varepsilon_{ij} \tag{3}$$

And it can be represented equally by the alternate forms:

$$J = \int_0^p \left(\frac{\partial \Delta}{\partial a}\right)_p dp = -\int_0^{\Delta} \left(\frac{\partial p}{\partial a}\right)_{\Delta} d\Delta \tag{4}$$

Where Δ is the work producing of load point displacement for the load, P. In the analysis, it is convenient to divide J-integral into elastic and plastic parts, J_{el} and J_{pl}. then the J-integral form in Equation (4) may be written:

$$J = J_{el} + J_{pl}$$

$$J = \int_0^p \left(\frac{\partial \Delta_{el}}{\partial a}\right)_p dp + \int_0^p \left(\frac{\partial \Delta_{pl}}{\partial a}\right)_p dp \tag{5}$$

The first item in the Equation (5) is the linear-elastic component and the second term is nonlinear-plastic component. The second term in Equation (5) can be reinterpreted by referring to Figure 2. This Figure shows the load-displacement curve for two different crack sizes *a* and *a+da*. The area between is noted to be Jp which is integrating over elements of the area by:

$$J_{pl} = \int_0^p \left(\frac{\partial \Delta_{pl}}{\partial a}\right)_p dp = -\int_0^{\Delta_{pl}} \left(\frac{\partial p}{\partial a}\right)_{\Delta_{pl}} d\Delta_{pl} \tag{6}$$

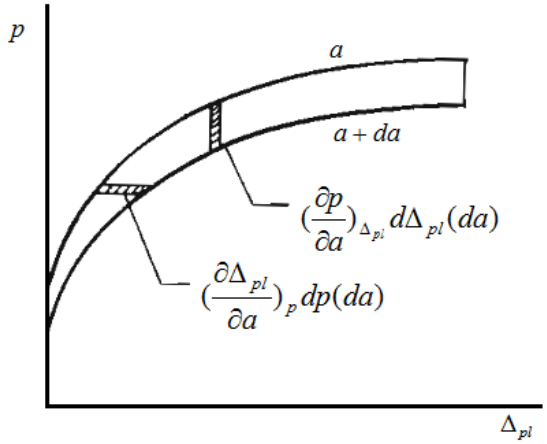

Figure 2. Load displacement for two different crack lengths

An important feature of the *J*-integral is that it is path independent and this helps to calculate the *J*-integral in a far distance from the crack tip. If Γ is considered as path-independent around an inclined crack tip which has angle of α with the x-axis, then *J*-integral will be can be shown in matrix form as:

$$J = \int_{\Gamma} W d\eta - \int_{\Gamma} \{\sigma_n \quad \tau_n\} \begin{bmatrix} \frac{\partial u_n}{\partial \xi} \\ \frac{\partial u_n}{\partial \xi} \end{bmatrix} ds \tag{7}$$

σ_n, and τ_n are the stresses in an arbitrary direction which has angle of α with x-axis.

$$\sigma_n = \sigma_{xx} \cos^2 \alpha + \sigma_{yy} \sin^2 \alpha + \tau_{xy} \sin \alpha \cos \alpha$$
$$\tau_n = (\sigma_{yy} - \sigma_{xx}) \sin \alpha \cos \alpha + \tau_{xy} (\cos^2 \alpha - \sin^2 \alpha) \tag{8}$$

u_n, and v_n are displacement in the same direction:

$$u_n = u \cos \alpha + v \sin \alpha$$
$$V_n = -u \sin \alpha + v \sin \alpha \tag{9}$$

Substituting Equations (8) and (9) in Equation (7) the *J*-integral will be easily calculated. Figure 3 shows that $Q_1Q_2Q_3Q_4$ can be considered as a path for calculating the *J*-integral in a fully elastic domain.

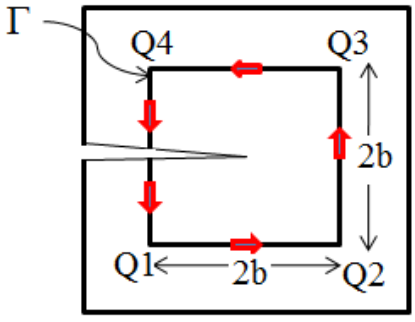

Figure 3. *J*-integral Path at the Crack Tip

First, the shape of the integral path is described and then value of integral is calculated on each separate path for two plane stress and plane strain condition. It is obvious that stress is $\sigma = D.\varepsilon$ in elastic condition and it can be stated in matrix form:

$$\begin{Bmatrix} \sigma_{xx} \\ \sigma_{yy} \\ \sigma_{xy} \end{Bmatrix} = \begin{bmatrix} D_{11} & D_{12} & 0 \\ D_{12} & D_{22} & 0 \\ 0 & 0 & D_{11} \end{bmatrix} . \begin{Bmatrix} \varepsilon_{xx} \\ \varepsilon_{yy} \\ \varepsilon_{xy} \end{Bmatrix} = \begin{bmatrix} D_{11}\varepsilon_{xx} + D_{12}\varepsilon_{yy} \\ D_{12}\varepsilon_{xx} + D_{22}\varepsilon_{yy} \\ D_{33}\varepsilon_{xy} \end{bmatrix} \tag{10}$$

Then strain energy density is calculated from:

$$W = \frac{1}{2}\sigma^T \varepsilon \tag{11}$$

Substituting Equation (10) in Equation (11), strain energy density will be:

$$W = \frac{1}{2}\varepsilon_{xx}\left(D_{11}\varepsilon_{xx} + D_{12}\varepsilon_{yy}\right) + \frac{1}{3}\varepsilon_{yy}\left(D_{12}\varepsilon_{xx} + D_{22}\varepsilon_{yy}\right) + \frac{1}{2}D_{33}\varepsilon_{xy}^2$$

$$W = \frac{1}{2}D_{11}\varepsilon_{xy}^2 + \frac{1}{2}D_{22}\varepsilon_{yy}^2 + D_{12}\varepsilon_{xx}\varepsilon_{yy} + \frac{1}{2}D_{33}\varepsilon_{xy}^2 \tag{12}$$

And the *J*-integral on the closed path is:

$$J = \int Q_1 Q_2 + \int Q_2 Q_3 + \int Q_3 Q_4 + \int Q_4 Q_1 \tag{13}$$

3 Finite Element Model

The finite element program ANSYS was used to simulate the tensile test on the steel plates with edge crack. One half of the sample was modeled, as shown in Figure 4b. The model considered the measured geometry, material properties and initial edge crack at the middle of the plate. A total 13045 quadratic plane strain elements are used throughout the entire domain with a mesh size of 0.01×0.01. Fine meshing is located near the crack tip of the sample where the intensity of the stress is expected to be larger. The stress distributions were calculated at desired applied loads. Ideal boundary conditions were chosen. A cubic steel plate is selected with dimensions of 1.5×0.5 in^2 and thickness of 0.25 inch. An edge crack is considered with lengths of 0.2 and 0.4 inch in the middle of the plate. A tensile force of 3640 lbs is applied at the bottom and the top of the plate. Figures 5 and 6 show the stress and displacement contour in Y-direction throughout the plate. Figure 5 shows the J-integral curve versus crack lengths which has been drawn using ANSYS. Figure 5 indicates an exponential relation between the crack length and J-integral. Equation (14) is dominant between crack lengths and J-integral for the ASTM A633 grade high-strength low-alloy (HSLA) steel plate specimens with edge crack at the middle.

$$J = 4292.2 \times e^{10.561a} \tag{14}$$

where *a* is length of the crack as shown in Figure 4a.

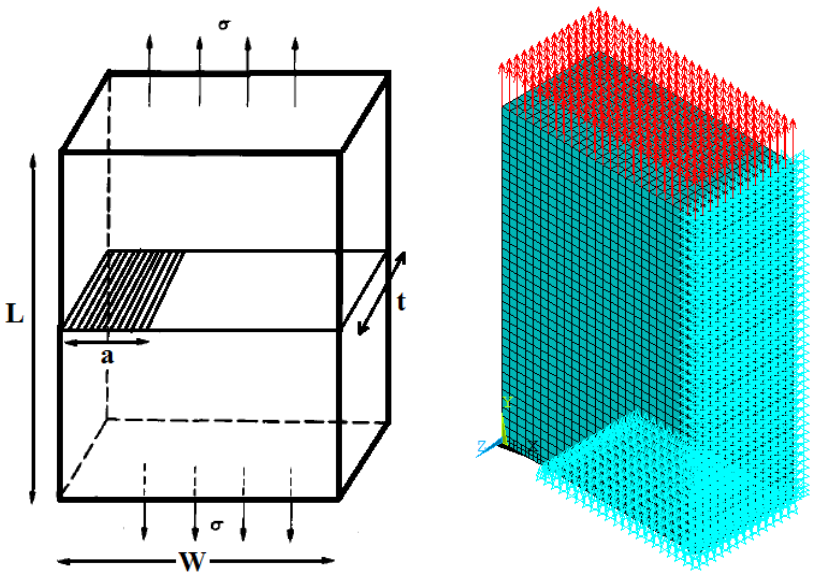

(a) (b)

Figure 4. 3-dimensional Crack Modeling in ANSYS

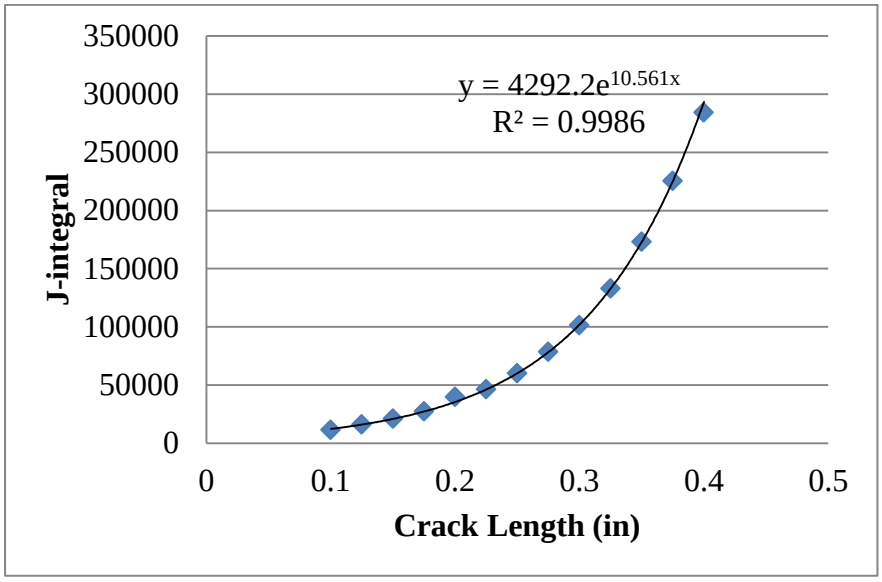

Figure 5. J-integral Curve for Different Crack Lengths

4 Experimental Works

Two steel samples are tested using a high capacity universal testing machine. The tests are running at a constant displacement rate of 0.03 inch/sec. Width of the plates are 0.5 in and length of them is 1.5 in with 0.25 in thicknesses. Width of the crack is 0.1 inch for the first sample and 0.2 inch for the second sample as shown in Figure 6.

Figure 6. Specimen A1 (a=0.2W), A2 (a=0.4W)

Steel specimens with an edge crack are tested using a universal testing machine (MTS 858 Mini-Bionix) at FIU's Material Laboratory. This machine designed for accurate testing under axial loads (tensile and compression testing) up to 3370 lbs (15 KN) with standard displacements of 3.94 in (100 mm) as shown in Figure 7. The steel material is ASTM A633 HSLA. Yielding strength for structural steel A633 HSLA is 63.1 ksi (435 MPa) and ultimate strength is 79.7 ksi (549 MPa). The plate was tested with rate of 0.03 inch/sec and maximum force of 2920 lbs (13 KN). Figure 8 shows the force versus displacement for this plate. It shows that sample A1 with edge crack length of 0.2W fractured around 7000 lbs and sample A2 with edge crack length of 0.4W fractured around 5500 lbs. Until 2000 lbs loading both samples have the same behavior.

Figure 7. Tensile Testing Machine

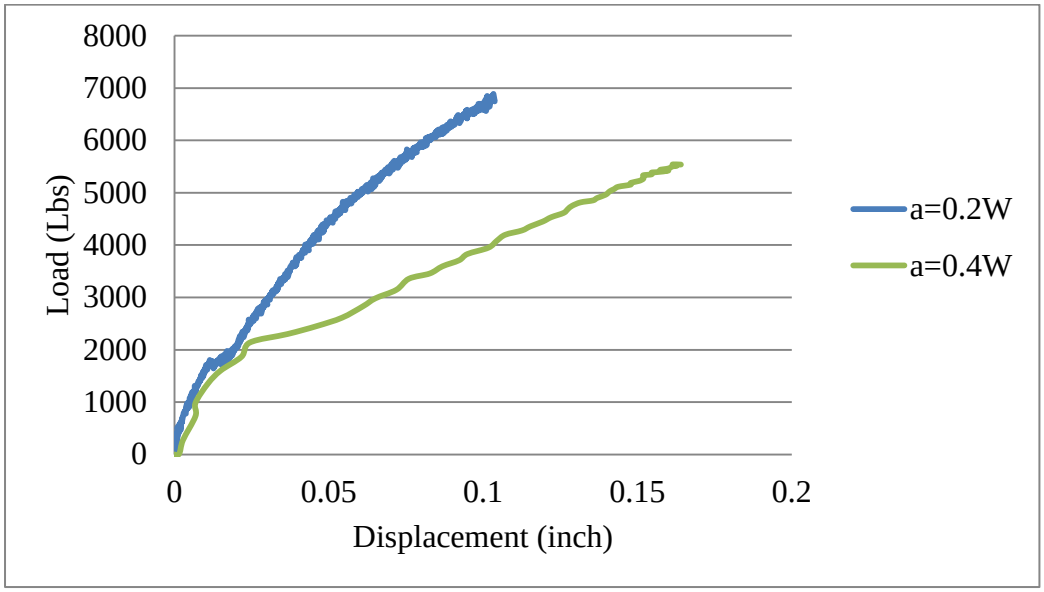

Figure 8. Load-displacement Curve, Experimental Result

5 Results of Microscopic Observations

In this part, Phenom microscope is used to get the best images from the crack tip surface of the fractured sample after performing tensile test. Sample needs to be dry before use and be firmly attached to the stub and the sample needs to be sprayed with compressed gas to remove any loose debris. The steel specimens are needed to be polished before using microscope to see the deformation of the crack tip. Metal polishes are performed in order to remove tarnish and lubricate the surface of the steel piece so that it can be observed to its original state. Polishes help metal to avoid damage to the surface. Usually, chemical liquid and paste such as ammonia, or alcohol are used in polishes for the metals.

Figure 9 shows the macroscopic configurations of both specimens after tensile test. Figures 9a and 9b show the fracture surface for sample A1. Figures 9c and 9d show the fracture surface for sample A2. For both samples, flaws initiates from the center of the crack tip at the middle of the specimen and propagate along the tensile direction to the regions close to end of the specimen.

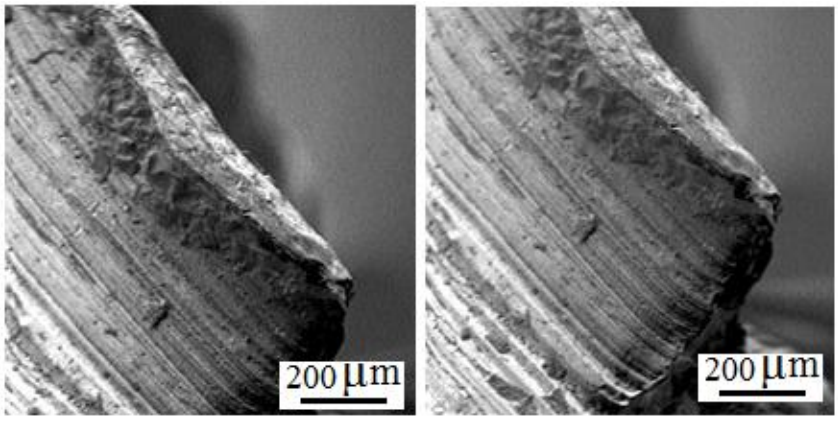

(a) (b)

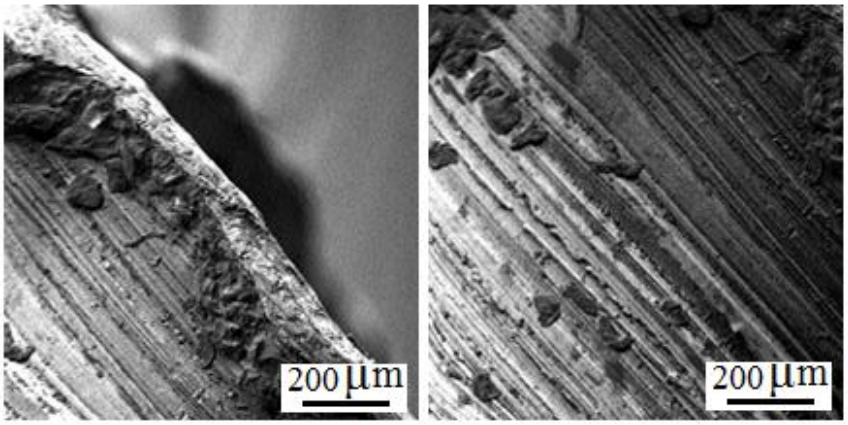

(c) (d)

Figure 9. Macroscopic Configuration and Fracture Surface of Steel Specimens (200µm)

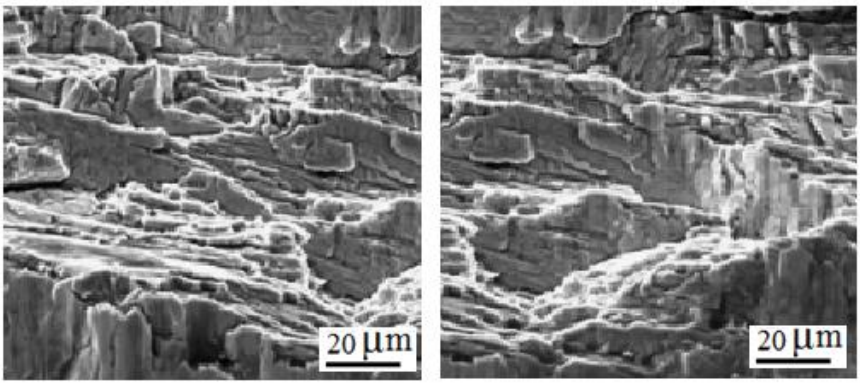

Figure 10. Macroscopic Configuration and Fracture Surface of Steel Specimens (20µm)

Conclusions

Tensile properties are almost the same for both specimens, cut in transverse and along thickness. With crack length increasing, yield strength, the ultimate tensile strength, and fracture stress show a decreasing trend. With increasing the applied load the two inclined shear cracks propagate to the center line where they are connected by shearing the longitudinal ligament. It is further revealed that the shear cracking inclined with an angle near 45° at both ends and parallel to the crack direction in the middle of specimens in all range of applied strain rates. Figures 10 shows the micro-features of the fracture surfaces of specimens. After samples had fractured, the surface of the steel was rough and irregular. The second half of the fractured sample showed a cup shape with an inclination of approximately 45° on their fracture surfaces. In a uniaxial tensile test, this orientation represents the angle of principle shear stress and the surface demonstrates this principle shear stress caused the crystalline boundaries to slip over each other before failure.

References

Ashby, M. (2006). “Engineering Materials 1: An Introduction to Properties, Applications and Design. ” 3 rd ed. Butterworth-Heinemann.

Cao, R., Li, L., Chen, J.H., Zhang, J., (2010). “Study on compression deformation, damage and fracture behavior of TiAl alloys Part II. Fracture behavior.”, Materials Science and Engineering A 527 2468–2477.

Kardomateas, G.A. (1986). “Fractographic Observations In Asymmetric And Symmetric Fully Plastic Crack Growth.” Pergamon Press Ltd., Vol.20, pp. 609-614.

Vinnakota, S. (2006). “Steel Structures: Behavior and LRFD.” 1 st Edition, pp. 29-46.

Askeland, D. R. (1984). “The Science and Engineering of Materials.” PWS Engineering, 1984, pp.151-259.

Wulff, J., et. al, “Structures and Properties of Materials.” Vol. 1, pp. 148-178.

Jin, X.; Li, G.; Aluru, N. R. (2001). “On the equivalence between least-squares and kernel approximations in meshless methods.” Computer Modeling in Engineering and Sciences, vol. 2, pp. 447-462.

Liu, W. K., Jun, S., Zhang, Y. F. (1995). “Reproducing Kernel Particles Methods.” International Journal for Numerical Methods in Fluids, vol. 20, pp. 1081-1106.

Du W. S., Cao, R., Yan, Y.J., Tian, Z. L., Peng, Y., Chen, J.H. (2007). “Fracture behavior of 9% nickel high-strength steel at various temperatures: Part I. Tensile tests, Materials Science and Engineering, Volume 486, Issues 1–2, 15 July 2008, Pages 611–625.

Meyers MA. (1994). “Dynamic behavior of materials” New York: Wiley.

Kaltho! JF, Gregor M. (1997). “Instrumental impact testing of subsize Charpy V-notch specimens.” In: Corwin WR, Rosinski ST, van Walle E, editors. Small specimen test techniques: ASTM STP. p. 1329.

Wei, X.C., Xu, L.P. , Fu, R.Y. , Lin, L.S, (2002). “Proceedings of the International Conference on TRIP-Aided High Strength Ferrous Alloys.” Ghent, June, p. 253.

Xia L, Shih F, Hutchinson JW, (1995). “A computational approach to ductile crack growth under large-scale yielding conditions.” J Mech Phys Solids, 43:389–413.

Simonsen BC, Lauridsen LP, (2000). “Energy absorption and ductile failure in metal sheets under lateral indentation by a sphere.” Int J Impact Eng, 24:1017–39.

Grønwold E. (2003). “Experimental set-up for large-scale fracture mechanics testing.” Master thesis, Department of Mechanical Engineering, Maritime Engineering, Technical University of Denmark.